

Order by quenched disorder in the model triangular antiferromagnet $\text{RbFe}(\text{MoO}_4)_2$

A. I. Smirnov,¹ T. A. Soldatov,^{1,2} O. A. Petrenko,³ A. Takata,⁴
T. Kida,⁴ M. Hagiwara,⁴ A. Ya. Shapiro,⁵ and M. E. Zhitomirsky⁶

¹*P. L. Kapitza Institute for Physical Problems, RAS, 119334 Moscow, Russia*

²*Moscow Institute for Physics and Technology, 141700 Dolgoprudny, Russia*

³*Department of Physics, University of Warwick, Coventry CV4 7AL, United Kingdom*

⁴*Center for Advanced High Magnetic Field Science (AHMF), Osaka University, Osaka 560-0043, Japan*

⁵*A. V. Shubnikov Institute for Crystallography RAS, 119333 Moscow, Russia*

⁶*CEA, INAC-PHELIQS, F-38000 Grenoble, France*

(Dated: September 27, 2018)

We observe a disappearance of the $1/3$ magnetization plateau and a striking change of the magnetic configuration under a moderate doping of the model triangular antiferromagnet $\text{RbFe}(\text{MoO}_4)_2$. The reason is an effective lifting of degeneracy of mean-field ground states by a random potential of impurities, which compensates, in the low temperature limit, the fluctuation contribution to free energy. These results provide a direct experimental confirmation of the fluctuation origin of the ground state in a real frustrated system. The change of the ground state to a least collinear configuration reveals an effective positive biquadratic exchange provided by the structural disorder. On heating, doped samples regain the structure of a pure compound thus allowing for an investigation of the remarkable competition between thermal and structural disorder.

Triangular-lattice antiferromagnets (TLAF) form a popular class of magnetic materials that provides paradigmatic cases of magnetic frustration [1] and intrinsic multiferroicity [2, 3]. A spectacular manifestation of frustration in TLAFs is the $1/3$ magnetization plateau with the up-up-down (*uud*) spin structure stabilized by fluctuations out of a degenerate manifold of classical ground states [4–6]. A $1/3$ magnetization plateau has been experimentally observed in a number of TLAFs [7–11]. Generally, it is a challenging task to distinguish the pure frustration-driven plateaus from those produced by additional perturbations, such as an Ising anisotropy or magnetoelastic coupling. The latter mechanism is responsible for the $1/2$ magnetization plateau in chromium spinels [12–14], whereas an Ising anisotropy may contribute to the $1/3$ plateau in some triangular antiferromagnets [9, 10]. Thus, a direct verification of the plateau mechanism remains a pressing issue in the field of frustrated magnetism.

An experimental test to determine if fluctuations are at the origin of the magnetization plateau states in TLAFs has recently been suggested [15]. It was shown theoretically that the frustration-driven plateaus become unstable in the presence of a weak structural disorder either in the form of nonmagnetic dilution or as an exchange-bond randomness. Weak disorder in frustrated magnets makes an energetic selection among degenerate ground states that competes with the effect of thermal or quantum fluctuations. Besides the plateau smearing, in fields below the plateau, the structural disorder may also stabilize umbrella- or fan-type magnetic structures instead of the more collinear states selected by fluctuations in clean TLAFs [4–6]. The strong influence of a weak doping is due to a high degree of degeneracy in a magnet with a fluctuation-selected ground state and will not

give a comparable effect in systems with a pronounced minimum of the mean-field energy. Thus the experimental observation of the plateau vanishing and of a ground state changing on doping serves as direct evidence of the fluctuation origin of corresponding phases in pure crystals with magnetic frustration. At the phenomenological level, the effect of structural disorder on degeneracy lifting in frustrated magnets may be represented by an effective biquadratic exchange with a positive sign [15–19]. In a different context, a positive biquadratic exchange was shown to be generated by surface roughness in ferromagnetic multilayers [20], where it leads to the experimentally observed 90° orientation of magnetizations [21, 22].

Our work is motivated by a search for direct experimental evidence for a disorder-induced positive biquadratic exchange in bulk frustrated magnets. We also seek to verify experimentally the fluctuation nature of the ground state of a pure TLAF and to observe the competition between static and dynamic disorder. The material chosen for the study is $\text{RbFe}(\text{MoO}_4)_2$, a magnetic compound featuring triangular-lattice layers of Fe^{3+} ions with semiclassical $S = 5/2$ spins. The system has an easy-plane magnetic anisotropy with the plane parallel to layers and exhibits a $1/3$ magnetization plateau only for $H \perp c$ (the c axis is normal to the Fe^{3+} layers) [23, 24]. Random exchange-bond modulations in triangular layers is achieved by substituting K for Rb in the interlayer space. In this Letter we present experimental results that demonstrate a rapid disappearance of the plateau on K-doping, whereas the Néel temperature T_N , the saturation field H_{sat} , and the antiferromagnetic resonance gap Δ are all changed by less than 15%. Furthermore, the electron spin resonance (ESR) measurements also reveal a drastic change of the spin structure with doping at fields below

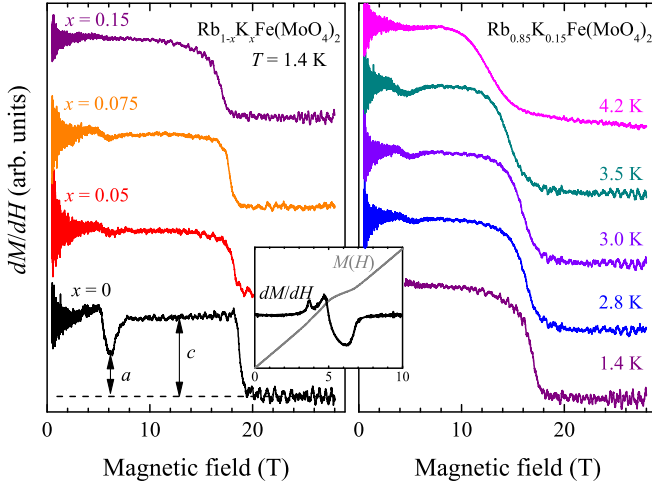


FIG. 1. (Color online) Left, dM/dH vs field curves for the $\text{Rb}_{1-x}\text{K}_x\text{Fe}(\text{MoO}_4)_2$ crystals with different x , measured in the pulse field $\mathbf{H} \perp c$ at $T = 1.4$ K. Parameters a and c are used to define a plateau *quality factor* Q (see main text). Inset, $M(H)$ and $dM(H)/dH$ curves taken for a pure sample at the same temperature in steady fields using a vibrating sample magnetometer. Right, dM/dH vs field curves for the $x = 0.15$ sample measured in the pulsed field $\mathbf{H} \perp c$ at different temperatures.

the plateau.

The crystals of $\text{Rb}_{1-x}\text{K}_x\text{Fe}(\text{MoO}_4)_2$ were prepared as previously described [8]. In addition to a controlled amount of K, about 1 atomic percent of Al was also found in some samples. This aluminum impurity, probably comes from the corundum crucible and is a likely reason for the observed dispersion in T_N of about ± 0.2 K for the samples with the same x . In the limiting case of $\text{KFe}(\text{MoO}_4)_2$ ($x=1$) we get a $\sim 50\%$ reduction of the principal exchange constant [25]. The magnetization curves $M(H)$ and susceptibility were studied by means of the vibrating sample magnetometer in magnetic fields up to 10 T and by a pulsed field method in the 30 T range using the 55 T magnet at the AHMF center in Osaka University. Multifrequency 25–150 GHz ESR was used to determine zero-field energy gap in AHMF center and to derive frequency-field diagrams and angular dependencies of ESR absorption in Kapitza Institute.

The magnetization plateau for the pure sample (as illustrated in the inset of Fig. 1) is clearly marked by a significant reduction in the derivative, dM/dH , measured for $\mathbf{H} \perp c$. The development of the $dM(H)/dH$ curves on doping is presented in the left panel of Fig. 1. At $T = 1.4$ K the decrease in the dM/dH value on the plateau becomes smaller with doping, and for $x = 0.15$ the plateau completely disappears. However, the temperature evolution of $dM(H)/dH$ curves for this $x = 0.15$ sample shows, that the plateau is restored, at least partially, on heating. The local minimum in the derivative appears again near 6 T for $T = 2.8$ K and remains clearly

visible at 3.0 and 3.5 K, as shown in Fig. 1, right panel. We present here only the records of the $dM(H)/dH$ curves for decreasing magnetic field, as this sweep direction helps to avoid the sample heating caused by a magnetocaloric effect. The full collection of the $dM(H)/dH$ curves for both increasing and decreasing fields is given in Supplemental Material [26].

We introduce a *quality factor*, $Q = 1 - a/c$, to characterize the magnetization plateau. Here a is the value of the dM/dH at its minimum on a plateau and c is the value of the dM/dH for the fields between the plateau and magnetization saturation, as defined in Fig. 1. For an ideal, perfectly flat plateau $Q = 1$, while $Q = 0$ corresponds to the absence of the plateau. The dependence of Q on doping and temperature (see Fig. 2) shows a disappearance of the plateau on doping and its restoration on heating. The value of H_{sat} is defined as a field where dM/dH decreases by 50% compared to its value just above a plateau. The value of $\mu_0 H_{\text{sat}}$ measured at $T = 1.4$ K decreases on doping from 18.6 T in a pure sample to 16.7 T for $x = 0.15$. An empirical width of the field transition to a saturation, estimated as a field interval where the dM/dH varies between 0.75 and 0.25 of the maximum value is 0.3 T for the $x = 0$ sample, and it increases to about 1.0 T for the $x = 0.15$ sample, but is still much smaller than the saturation field itself. Using a similar criterion, that the change of derivative dM/dT varies between 0.75 and 0.25 of the maximum value, the transition width ΔT at T_N can also be estimated. ΔT is about 0.1 K for all x , except $x = 0.05$ where it is 0.3 K, thus showing that the transition region is significantly smaller than T_N . On doping, the value of T_N decreases from 4.1 K for $x = 0$ to 3.0 K for the $x = 0.15$ sample. The x -dependencies of the normalized values of T_N and H_{sat} are presented in the left panel of Fig. 2.

The ESR spectra of a nominally pure sample (left panels of Fig. 3) have an energy gap of $\Delta_0 \simeq 90$ GHz and for $\mathbf{H} \perp c$ consist of the two frequency branches, ascending and descending with an applied magnetic field in agreement with the previous results [8, 24]. The ascending

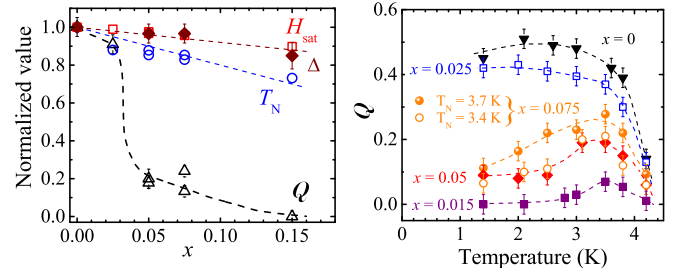


FIG. 2. (Color online) Left panel, normalized values of Néel temperature T_N , saturation field H_{sat} , excitation gap Δ and plateau quality factor Q vs doping. Right panel, plateau quality factor Q vs temperature for samples with different doping concentration. Dashed lines are guides to the eyes.

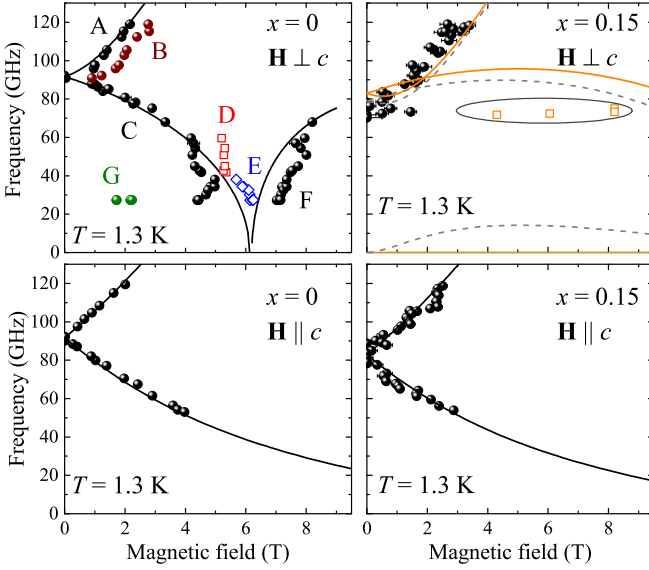


FIG. 3. (Color online) Frequency-field diagrams of the $\text{Rb}_{1-x}\text{K}_x\text{Fe}(\text{MoO}_4)_2$ samples for $x = 0$ (left-hand side panels) and $x = 0.15$ (right-hand side panels). The top and bottom panels show the ESR frequencies for $H \perp c$ and $H \parallel c$, respectively. The experimental results (symbols) are compared to the calculations (solid lines) for the Y/umbrella structure with $J = 1.1J_0$, $D = D_0$ for $x = 0$ and for the inverted Y (\bar{Y})/umbrella state with $J = 0.9J_0$, $D = D_0$ for $x = 0.15$, see main text for the notations. Dashed lines represent a calculation for the \bar{Y} state with $K/J = 0.01$, while the ellipse covers a wide area of a weak absorption.

branch is split into two closely-positioned branches, (A) and (B), by the weak interplane interactions. The frequency of the descending branch, (C), is reduced almost to zero for the field approaching the lower boundary of the plateau, while another mode, (D), of a higher frequency, appears near the entrance of the plateau. Modes in the middle of the plateau (E) and at the upper boundary (F) are also detected in qualitative agreement with the theory [6] and previous experiments [8]. Finally, a weakly-absorbing mode (G) near 30 GHz appears due to a splitting of the zero-frequency mode [8]. A full record of the microwave absorption *vs* magnetic field at different frequencies is given in Supplemental Material [26].

The frequency-field dependencies for the $x = 0.15$ sample are shown in the right-hand panels of Fig. 3. The gap Δ is reduced to (75 ± 5) GHz on doping, its evolution with doping concentration x is shown in Fig. 2. For a pure sample, ESR lines are observed both above and below Δ_0 for $H \perp c$ while for the $x = 0.15$ sample only the ascending ESR branch is detected. The descending ESR branch either disappears or transforms in a field-independent mode on doping. For the field, $H \parallel c$, both the ascending and descending branches are visible for pure and all doped samples, see lower panels in Fig. 3 and [26]. The angular dependence of the ESR absorption, presented in [26] reveals, that upon rotating from

$H \parallel c$ to $H \perp c$, the ESR line of the descending branch is smeared at a deviation from the c axis and disappears completely for $H \perp c$ in the $x = 0.15$ sample, while it is conserved in a pure sample. This observation gives a direct confirmation of the disappearance of the descending ESR branch on doping.

To model the observed behavior of doped $\text{RbFe}(\text{MoO}_4)_2$, we use the spin Hamiltonian

$$\hat{\mathcal{H}} = \sum_{\langle ij \rangle} J_{ij} \mathbf{S}_i \cdot \mathbf{S}_j + D \sum_i (S_i^z)^2 - g\mu_B \sum_i \mathbf{H} \cdot \mathbf{S}_i. \quad (1)$$

The nearest-neighbor exchange constant J_{ij} is assumed to have weak random variation between the bonds: $J_{ij} = \langle J_{ij} \rangle + \delta J_{ij}$, $\langle \delta J_{ij} \delta J_{kl} \rangle = \delta J^2 \delta_{ij,kl}$, $\delta J \ll J = \langle J_{ij} \rangle$. Inelastic neutron scattering experiments yield $J_0 = 0.086$ meV and $D_0 = 0.027$ meV for $\text{RbFe}(\text{MoO}_4)_2$ [27]. The effect of bond disorder and/or thermal and quantum fluctuations can be semi-quantitatively represented by adding a biquadratic term

$$\hat{\mathcal{H}}_B = K \sum_{\langle ij \rangle} (\mathbf{S}_i \cdot \mathbf{S}_j)^2. \quad (2)$$

For the purely Heisenberg model (1) with $D = 0$, $\delta J_{ij} = 0$, the quantum fluctuations contribute $K_Q \simeq -J/(24S^3)$ [28]. A negative sign for the biquadratic constant K means that fluctuations select the most collinear/coplanar states resulting in a standard sequence of the ordered states as the field increases, see Fig. 4(a)–(c) [6]. A frozen bond disorder instead generates a positive biquadratic contribution, $K_{\text{dis}} = \delta J^2/(3JS^2)$ [15]. For $(\delta J/J)^2 > 1/(8S)$, the disorder effect becomes dominant and the stable magnetic states are found by minimizing a Hamiltonian, which combines (1) and (2) with $K > 0$. One can straightforwardly verify that in such a case the least collinear states are energetically preferred. For the planar spin system ($D > 0$), this is the inverted Y

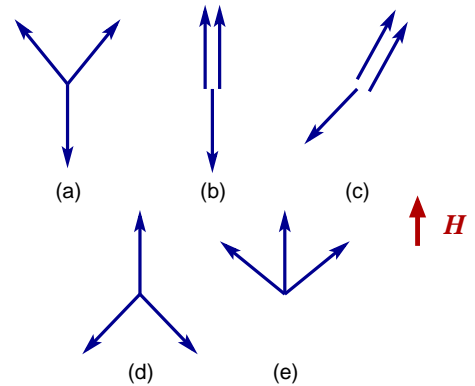


FIG. 4. Spin structures appearing for the pure TLAF in an applied field: (a) the Y state, (b) the *uud* state, (c) the 2:1 state. Spin structures of a planar triangular antiferromagnet in the presence of structural disorder: (d) \bar{Y} state and (e) the fan state.

(\bar{Y}) state, Fig. 4(d), which continuously transforms into the fan state in higher fields, Fig. 4(e). Small variations in the direction of the local anisotropy axis may also contribute to a lifting of the degeneracy and K_{dis} , but this weak effect is ignored as $D < J$.

The two possible low-field magnetic structures, the Y and the \bar{Y} states, have qualitatively different ESR spectra for in-plane orientations of an applied field. This fact fully agrees with the idea of an order-by-disorder effect, which relates the lifting of degeneracy in frustrated magnets to the excitation spectra of the different ground states [29, 30]. Performing the standard spin-wave calculations for (1) we obtain two two resonance frequencies:

$$\begin{aligned}\omega_1 &= 3JS\sqrt{d(1 \mp h)(3 \pm h)}, \quad d = \frac{D}{3J} \\ \omega_2 &= 3JS\sqrt{2d + h^2 + d(1 \pm h)^2}, \quad h = \frac{g\mu_B H}{3JS}, \quad (3)\end{aligned}$$

where the upper/lower sign corresponds to the Y/ \bar{Y} state. The third ESR branch vanishes in the harmonic approximation $\omega_3 = 0$ reflecting the remaining classical degeneracy.

For $H \perp c$, the ESR frequencies of pure $\text{RbFe}(\text{MoO}_4)_2$ shown in the upper left panel of Fig. 3, are accurately described by the expressions (12) for the Y state with $J = 1.1J_0$ and $D = D_0$, the values that are marginally different from the ones obtained in the neutron scattering experiments [27]. The agreement between theory and experiment is good despite presence of the incommensurate spiral state in low fields [3], which may indicate significant Y-type distortions of the spiral structure induced by an external field. The same microscopic parameters also nicely fit the ESR data for $H \parallel c$, the lower left panel of Fig. 3, see also [26]. The characteristic feature of the ESR spectra for the Y state ($H \perp c$) is the descending branch $\omega_1(H)$ that corresponds to the out-of plane oscillations of the two spin sublattices about the field direction, while the third sublattice remains parallel to the field. The frequency of this mode decreases to zero upon a transition into the collinear *uud* structure at $\mu_0 H \approx 6$ T. In contrast, the frequency of the same mode for the \bar{Y} state, which remains noncollinear, exhibits little variation in the corresponding field region. Thus, the absence of the descending ESR branch for the doped samples for $H \perp c$ clearly indicates a change of the spin structure. We compare the ESR data for the $x = 0.15$ doped sample with the theoretical frequencies (12) for the \bar{Y} state on the upper right panel in Fig. 3. A somewhat smaller averaged value of $J = 0.9J_0$ ($D = D_0$) used for the fit is consistent with a local reduction of the exchange interaction induced by K impurities.

The biquadratic interaction (2) has been derived as an effective potential in the manifold of degenerate classical ground states [28]. Nevertheless, the effect of structural disorder on the $q = 0$ excitations in the \bar{Y} state beyond substituting averaged J and D can be estimated by ex-

plicitly including $\hat{\mathcal{H}}_B$ in the calculations. One should bear in mind that an effective biquadratic interaction is rather weak. Using $K_{dis} = \delta J^2/(3JS^2)$ [15] and noting that the local $\delta J/J \simeq 50\%$, we find that the biquadratic constant does not exceed $K_{dis}/J = 0.01\text{--}0.02$, whereas $K_Q/J \simeq -3 \times 10^{-3}$. We show in the upper right panel of Fig. 3 the ESR modes computed for $J = 0.9J_0$, $D = D_0$, and $K/J = 0.01$. The main qualitative effect of $\hat{\mathcal{H}}_B$ is a nonzero value for ω_3 , which reflects a lack of degeneracy, whereas the shift of the two upper modes is indeed tiny. The resonance frequencies for the third branch are too small to be detected in the ESR spectrometers used here.

One can see in Fig. 2, that the plateau quality Q changes drastically with doping, whereas T_N , H_{sat} and Δ exhibit a weak linear dependence on x . The samples with the plateau suppressed or canceled by the impurities still demonstrate a sharp Néel transition, shifted down in temperature from T_N in a pure sample. The behavior of T_N , H_{sat} and Δ shows that the exchange interaction is not strongly affected on doping. A sharp Néel transition and a step-like change in dM/dH at saturation confirm the absence of the macroscopic inhomogeneities in the samples studied. Thus, the observed disappearance of the plateau and the change of the ground state in low fields should only be ascribed to the influence of a random potential. This statement is confirmed by the observed partial restoration of a plateau in doped samples on heating (see Fig. 2). Indeed, according to Ref. [15], the region of the *uud*-phase (1/3-plateau phase) in the $T - H$ phase diagram is shifted to a higher temperatures on doping.

In conclusion, the observed doping-induced changes of the magnetization curves and the magnetic resonance spectra of $\text{RbFe}(\text{MoO}_4)_2$ reveal a transition from a collinear up-up-down structure, stabilized by fluctuations, to a fan structure supported by a weak static disorder, as well a transformation of the lower-field spin structure from the Y-type to an inverted Y-structure. Our experiments establish the fluctuation origin of the 1/3-plateau and the Y-type phases and show that the ground state selection process is affected by a strong competition between structural disorder and thermal fluctuations. The structural disorder is found to lead to a positive biquadratic exchange. We observe a fundamentally different behavior between pure and lightly doped samples on heating, which results in the restoration of the magnetization plateau in the doped materials, while in a pure crystal the plateau is removed. These observations provide convincing confirmation of the competition between thermal and quenched disorder, demonstrating that the negative biquadratic term arising from thermal fluctuations once again dominates at higher temperature. Disorder-induced modifications of the magnetic structure may also be used to control multiferroicity of TLAf's and, perhaps, of other spiral antiferromagnets.

We thank S.S. Sosin and L.E. Svistov for numerous discussions. Work at the Kapitza Institute is supported by Russian Foundation for Basic Research, grant No. 15-02-05918, by the Programs of the Presidium of Russian Academy of Sciences, high-frequency ESR measurements are supported by Russian Science Foundation grant No. 17-12-01505. AIS is indebted to Osaka University for invitation as a visiting Professor. Work at Osaka University is supported by the International Joint Research Promotion Program.

-
- [1] M. F. Collins and O. A. Petrenko, *Can. J. Phys.* **75**, 605 (1997).
 - [2] H. J. Lewtas, A. T. Boothroyd, M. Rotter, D. Prabhakaran, H. Müller, M. D. Le, B. Roessli, J. Gavilano, and P. Bourges, *Phys. Rev. B* **82**, 184420 (2010).
 - [3] M. Kenzelmann, G. Lawes, A. B. Harris, G. Gasparovic, C. Broholm, A. P. Ramirez, G. A. Jorge, M. Jaime, S. Park, Q. Huang, A. Ya. Shapiro, and L. A. Demianets, *Phys. Rev. Lett.* **98**, 267205 (2007).
 - [4] D. H. Lee, J. D. Joannopoulos, J. W. Negele, and D. P. Landau, *Phys. Rev. Lett.* **52**, 433 (1984).
 - [5] H. Kawamura and S. Miyashita, *J. Phys. Soc. Jpn.* **54**, 4530 (1985).
 - [6] A. V. Chubukov and D. I. Golosov, *J. Phys.: Condens. Mat.* **3**, 69 (1991).
 - [7] T. Inami, Y. Ajiro, and T. Goto, *J. Phys. Soc. Jpn.* **65**, 2374 (1996).
 - [8] L. E. Svistov, A. I. Smirnov, L. A. Prozorova, O. A. Petrenko, L. N. Demianets, and A. Ya. Shapiro, *Phys. Rev. B* **67**, 094434 (2003).
 - [9] H. Kitazawa, H. Suzuki, H. Abe, J. Tang, and G. Kido, *Physica B* **259-261**, 890 (1999).
 - [10] R. Ishii, S. Tanaka, K. Onuma, Y. Nambu, M. Tokunaga, T. Sakakibara, N. Kawashima, Y. Maeno, C. Broholm, D. P. Gautreaux, J. Y. Chan, and S. Nakatsuji, *EPL* **94**, 17001 (2011).
 - [11] Yu. Shirata, H. Tanaka, A. Matsuo, and K. Kindo, *Phys. Rev. Lett.* **108**, 057205 (2012).
 - [12] H. Ueda, H. A. Katori, H. Mitamura, T. Goto, and H. Takagi, *Phys. Rev. Lett.* **94**, 047202 (2005).
 - [13] K. Penc, N. Shannon, and H. Shiba, *Phys. Rev. Lett.* **93**, 197203 (2004).
 - [14] H. Ueda, H. Mitamura, T. Goto, and Y. Ueda, *Phys. Rev. B* **73**, 094415 (2006).
 - [15] V. S. Maryasin and M. E. Zhitomirsky, *Phys. Rev. Lett.* **111**, 247201 (2013).
 - [16] C. L. Henley, *Phys. Rev. Lett.* **62**, 2056 (1989).
 - [17] M. W. Long, *J. Phys.: Condens. Mat.* **1**, 2857 (1989).
 - [18] Y. V. Fyodorov and E. F. Shender, *J. Phys. Condens. Matter* **3**, 9123 (1991).
 - [19] V. S. Maryasin and M. E. Zhitomirsky, *J. Phys.: Confer. Ser.* **592**, 012112 (2015).
 - [20] J. C. Slonczewski, *Phys. Rev. Lett.* **67**, 3172 (1991).
 - [21] S. O. Demokritov, *J. Phys. D* **31**, 925 (1998).
 - [22] C. M. Schmidt, D. E. Bürgler, D. M. Schaller, F. Meisinger, and H.-J. Güntherodt, *Phys. Rev. B* **60**, 4158 (1999).
 - [23] L. E. Svistov, A. I. Smirnov, L. A. Prozorova, O. A. Petrenko, A. Micheler, N. Büttgen, A. Ya. Shapiro, and L. N. Demianets, *Phys. Rev. B* **74**, 024412 (2006).
 - [24] A. I. Smirnov, H. Yashiro, S. Kimura, M. Hagiwara, Y. Narumi, K. Kindo, A. Kikkawa, K. Katsumata, A. Ya. Shapiro, and L. N. Demianets, *Phys. Rev. B* **75**, 134412 (2007).
 - [25] A. I. Smirnov, L. E. Svistov, L. A. Prozorova, A. Zheludev, M. D. Lumsden, E. Ressouche, O. A. Petrenko, K. Nishikawa, S. Kimura, M. Hagiwara, K. Kindo, A. Ya. Shapiro, and L. N. Demianets, *Phys. Rev. Lett.* **102**, 037202 (2009).
 - [26] See Supplemental Material for further experimental and theoretical details.
 - [27] J. S. White, Ch. Niedermayer, G. Gasparovic, C. Broholm, J. M. S. Park, A. Ya. Shapiro, L. N. Demianets, and M. Kenzelmann, *Phys. Rev. B* **88**, 060409 (2013).
 - [28] M. E. Zhitomirsky, *J. Phys.: Confer. Ser.* **592**, 012110 (2015).
 - [29] E. F. Shender, *Zh. Eksp. Teor. Fiz.* **83**, 326 (1982) [*Sov. Phys. JETP* **56**, 178 (1982)].
 - [30] R. Moessner, *Can. J. Phys.* **79**, 1283, (2001).

Supplemental Material for
 “Order by quenched disorder in the triangular
 antiferromagnet $\text{RbFe}(\text{MoO}_4)_2$ ”

SAMPLE PREPARATION AND CHARACTERIZATION

The crystals of $\text{Rb}_{1-x}\text{K}_x\text{Fe}(\text{MoO}_4)_2$ were prepared as previously described [1]. The K content was determined by means of energy-dispersive X-ray spectroscopy. The crystal structure was checked by powder and single crystal X-ray diffraction and confirmed the crystal group as $P3\bar{m}1$ with the room-temperature lattice parameters $a = 5.69 \text{ \AA}$ and $c = 7.48 \text{ \AA}$ for $x = 0$. The c axis exhibits a monotonic decrease with doping, for $x = 0.15$ this decrease is $(0.030 \pm 0.015) \text{ \AA}$.

A small amount of aluminum impurity, about 1 atomic percent, was also found in some samples. The aluminum impurity probably comes from the corundum crucible. Being random and uncontrolled, it is the likely reason for the observed dispersion of about 0.2 K in the Néel temperature for the samples with nominally the same content of K. For example, two nominally pure samples have different Néel temperatures: sample 1 with $T_N = (4.1 \pm 0.05) \text{ K}$ and sample 2 with $T_N = (3.7 \pm 0.05) \text{ K}$. Similarly, for the two samples with $x = 0.075$, the ordering temperature varies between 3.4 and 3.7 K.

EXPERIMENTAL RESULTS

Magnetization curves

The susceptibility *vs* temperature, $\chi(T)$, dependencies are shown in Fig. 1, the temperature dependence of the derivative $d\chi/dT$ is presented in Fig. 2. The susceptibility measurements were made with the magnetic field applied perpendicular to the c axis, where a kink of $\chi(T)$ clearly marks the Néel temperature T_N . The derivative $d\chi/dT$ has a negative sign at temperatures above the kink and is positive below the Néel point and, thus, shows a jump with a value of δ at the critical point. It is clearly seen in Fig. 1 that the Néel transition in doped samples is almost as sharp as in the pure samples. We estimate the width ΔT of the Néel transition as the temperature interval where the change of $d\chi/dT$ varies between 0.25 and 0.75 of the total jump δ . The width of the Néel transition is less than 0.3 K (see Fig. 2) for all doped and pure samples, which is small in comparison to the Néel temperature itself.

The 1/3 magnetization plateau, which is the remarkable feature of $\text{RbFe}(\text{MoO}_4)_2$, is observable at the in-plane ($\mathbf{H} \perp c$) orientation of the magnetic field, and is clearly marked by the drop of the derivative dM/dH near the field of $H_{\text{sat}}/3$, i.e. near 6 T. The dM/dH curves of a

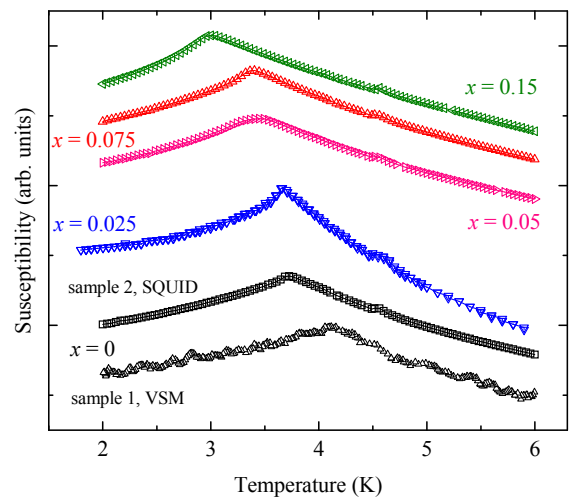


FIG. 1. Magnetic susceptibility *vs* temperature of $\text{Rb}_{1-x}\text{K}_x\text{Fe}(\text{MoO}_4)_2$ samples. The data for the $x = 0$, sample 1 are taken in a magnetic field of 0.05 T, while other curves are taken in a field of 0.1 T. The magnetic field is applied perpendicular to the c axis. The curves are vertically offset for clarity.

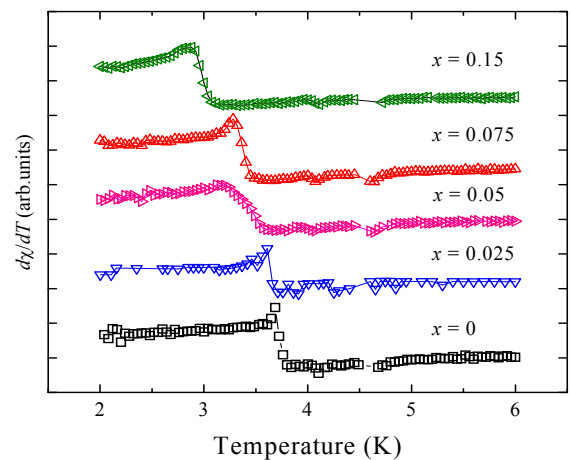


FIG. 2. Temperature derivative of the magnetic susceptibility, $d\chi/dT$ for the $\text{Rb}_{1-x}\text{K}_x\text{Fe}(\text{MoO}_4)_2$ samples with different doping concentration. The curves are offset for clarity.

nominally pure sample with $T_N = (4.1 \pm 0.05) \text{ K}$ recorded in a pulsed field in the whole range including the saturation field 18.6 T are presented in Fig. 3 and are analogous to those previously observed in Ref. [2]. The duration of the pulse of the magnetic field is 7 ms.

The changes in the magnetization curves, which arise at intermediate doping of $x = 0.075$, are shown in Fig. 4: here we see, that at the lowest temperature 1.4 K, the drop of dM/dH in the plateau range is much smaller than in the pure sample. Nevertheless, the plateau still remains observable, in contrast to the sample with $x = 0.15$, where it disappears completely at $T = 1.4 \text{ K}$ (see main text). The temperature dependencies of dM/dH

curves for $x = 0.075$, presented in Fig. 4 demonstrate that the plateau, marked by a drop of the derivative near 6 T, is restored by an increase in the temperature. At a temperature of about 3 K the plateau is again well pronounced: the drop of dM/dH is about a half of that of a pure sample, while at $T = 1.4$ K this drop is only one sixth of the drop in a pure sample.

The plateau recorded in the pulsed field usually has a Q -value (see definition of Q in the main text), which is 10-20% lower than that recorded by the vibrating sample magnetometer in a steady field. This is probably due to a finite time resolution of the recording system and a finite relaxation time of the spin system. Sweeping through the field interval of 0.2 T at the plateau entrance, where dM/dH is quickly changing, takes about 15 μ s, this may be comparable or several times longer, than the relaxation time of the spin system of an antiferromagnet. The hysteresis of the dM/dH curves near the saturation field is due to the magnetocaloric effect, as described in Ref. [2]. Due to the magnetocaloric effect the sample is slightly heated during the magnetization process, while during the demagnetization it is cooled. Because of this, we observe a larger saturation field when the field is reduced from the maximum value to zero, than during the field sweep from zero to the maximum value. The saturation fields and values of the plateau quality Q are quoted for the “down”-records of dM/dH .

Electron spin resonance

Electron spin resonance (ESR) absorption lines were recorded as magnetic field dependencies of the microwave

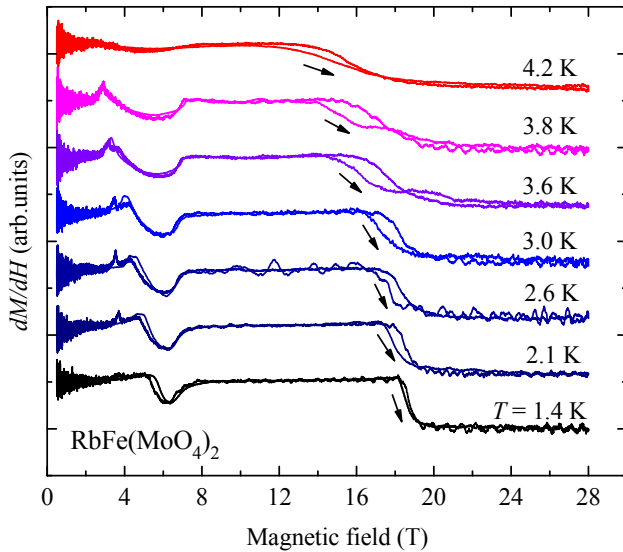


FIG. 3. Magnetization derivative curves dM/dH for a pure $\text{RbFe}(\text{MoO}_4)_2$ sample measured in a pulsed field for $\mathbf{H} \perp c$. Both increasing and decreasing field records are shown.

power, transmitted through the resonator with the sample. The diminishing of this transmission indicates an increase in the absorption. A small amount of diphenylpicryl-hydrazyl (DPPH) was used to mark the ESR field of free spins at the Larmor frequency $f_L = 2\mu_B H/h$. Figure 5 presents a comparison of the 26.9 GHz ESR absorption lines for a pure and two doped samples with $x = 0.075$ and 0.15 at the lowest temperature $T = 1.3$ K. At this frequency the pure sample exhibits three resonances marked as C, E, F (the labels are the same as in the frequency-field diagram of Fig. 3 in the main text) in the plateau range, while for $x = 0.075$ these modes are of much lower intensity and for $x = 0.15$ they disappear completely, analogous to the plateau itself.

Figure 6 presents the temperature evolution of the ESR absorption of the $x = 0.15$ sample at a frequency of 26.9 GHz. We see that the absorption features, suppressed by doping for low temperature, are partially restored by heating above 2 K, analogous to the restoring of the plateau observed in the magnetization measurements described in the main text. On heating above the Néel temperature, the ESR line transforms into a regular Lorentzian absorption curve at the resonance field of the Larmor precession 0.96 T.

A comparison of ESR responses of pure and doped ($x = 0.15$) samples at different frequencies f is presented for the in-plane magnetic field in Fig. 7. These records enable one to reconstruct the $f(H)$ dependencies, presented in Fig. 3 in the main text. Figure 7 illustrates the disappearance of the descending branch of the antiferromagnetic resonance spectrum in the $x = 0.15$ sample. Indeed, we can see that the ESR lines are clearly

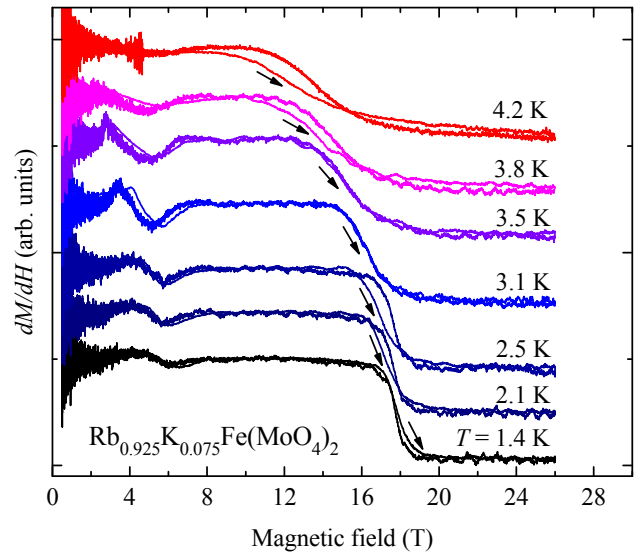


FIG. 4. Magnetization derivative curves dM/dH for the $\text{Rb}_{1-x}\text{K}_x\text{Fe}(\text{MoO}_4)_2$ sample with $x = 0.075$ measured at different temperatures in a pulsed field for $\mathbf{H} \perp c$. Both increasing and decreasing field records are shown.

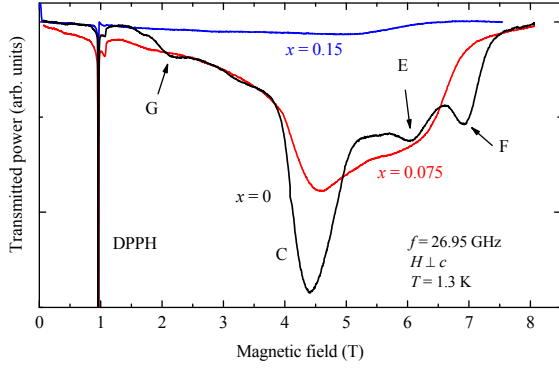


FIG. 5. Normalized ESR absorption curves ($\mathbf{H} \perp c$) for the $\text{Rb}_{1-x}\text{K}_x\text{Fe}(\text{MoO}_4)_2$ samples with $x = 0, 0.075$ and 0.15 .

pronounced at frequencies below the 90 GHz gap for a pure sample. At the same time, there are no visible resonance lines at the frequency below the 75 GHz gap for the $x = 0.15$ sample. On heating both the pure and the doped samples to a temperature of about 10 K, the Larmor frequency line of the same amplitude appears in both cases. At a frequency below the gap for the doped sample (75 GHz), the record of the microwave power transmitted through the resonator does not have a resonance shape and demonstrates only a weak variation of transmitted signal with magnetic field, see Fig. 8. This is to be compared with pronounced ESR lines of the descending branch of the pure sample or of the doped sample for $\mathbf{H} \parallel c$.

For the magnetic field directed perpendicular to the planes of magnetic layers (i.e. $\mathbf{H} \perp c$), we observe the ascending and descending branches both for the pure and the most highly doped $x = 0.15$ samples, see Fig. 9. To confirm the phenomenon of the disappearance of the descending branch for $\mathbf{H} \perp c$, we studied the evolution of

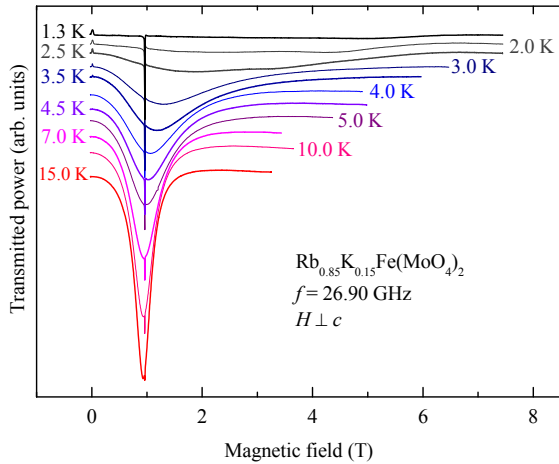


FIG. 6. Temperature evolution of the ESR absorption curve for the $\text{Rb}_{0.85}\text{K}_{0.15}\text{Fe}(\text{MoO}_4)_2$ sample with $x = 0.15$. Narrow ESR signal in a magnetic field of 0.96 T is a DPPH marker.

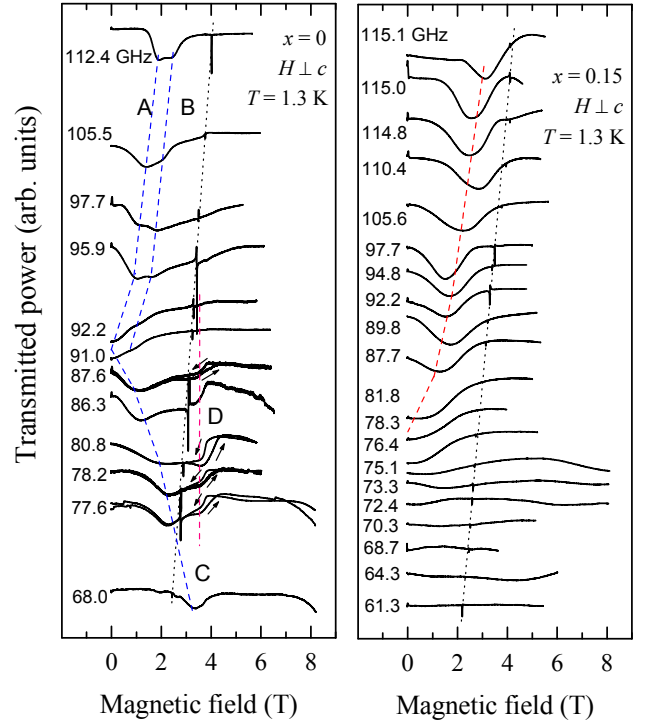


FIG. 7. Normalized ESR absorption curves for the in-plane magnetic field for $\text{Rb}_{1-x}\text{K}_x\text{Fe}(\text{MoO}_4)_2$ samples with $x = 0$ and 0.15 for different frequencies. The gain is normalized to the intensity of the paramagnetic resonance signal at $T = 10$ K. Dashed lines in left panel are guides to the eye: blue lines are for the AB-doublet of the ascending mode and for the descending mode C, black line is a DPPH label, red line is mode D at the right boundary of the plateau range. Dashed lines in the right panel are guides to the eye for the ascending branch (red line) and for a DPPH mark (black line).

ESR records while gradually rotating the magnetic field from the $\mathbf{H} \parallel c$ orientation to the in-plane orientation at a frequency below the gap for the pure sample and for the $x = 0.15$ sample. The results are presented in Fig. 10. One can see here, that for the doped sample the ESR line is smeared on rotation and is transformed into a curve which does not have a resonance shape and demonstrates only a weak variation with magnetic field. At the same time, for the pure sample, the resonance absorption curve of the descending ESR mode survives the process of a rotation. The increase of the linewidth of the pure sample, observed as a result of the rotation of the magnetic field to the in-plane direction may be naturally explained by the decrease of the absolute value of df/dH from $\mathbf{H} \parallel c$ to $\mathbf{H} \perp c$, as observed in Ref. [2].

For the families of ESR curves presented in Figs. 7, 9 and 10 the gain is adjusted to keep the integrated intensity of the ESR signal at $T = 10$ K equal for all frequencies. This ensures that the records made at different frequencies and at different positions in the resonator are taken at the same sensitivity to microwave absorption in

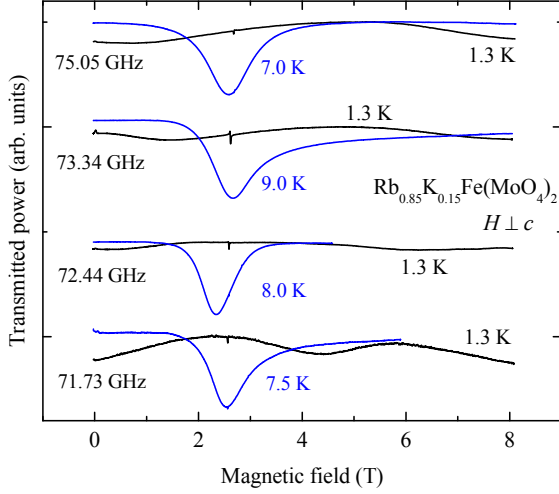


FIG. 8. Weak microwave absorption in the vicinity of 74 GHz in the $x = 0.15$ sample for $\mathbf{H} \perp c$ and $T = 1.3$ K (black lines). Blue lines show the microwave transmission at higher temperature, with the same gain of a detector circuit. Narrow ESR signals are from a DPPH marker.

the sample.

The ESR absorption demonstrates a distinct difference in angular dependence of the lower branch for the pure and doped samples. This shows the disappearance of the low-frequency absorption on rotation of the magnetic field in a doped sample, while for the pure sample this branch survives both for the in-plane and out-of plane fields.

THEORY

We present here the calculation of the ESR spectrum for the conical/umbrella state which have been used to describe the experimental results for $\text{RbFe}(\text{MoO}_4)_2$ for magnetic fields applied along the c axis. We use the nearest-neighbor spin Hamiltonian without bond disorder:

$$\hat{\mathcal{H}} = J \sum_{\langle ij \rangle} \mathbf{S}_i \cdot \mathbf{S}_j + D \sum_i (S_i^z)^2 - g\mu_B \sum_i \mathbf{H} \cdot \mathbf{S}_i. \quad (1)$$

For the easy-plane anisotropy and $\mathbf{H} \parallel \hat{\mathbf{z}}$ spins form the conical state described by the rotation angle $\theta_i = \mathbf{Q} \cdot \mathbf{R}_i$ in the x - y plane and by the out of plane tilting angle α . The transformation between the laboratory frame x_0, y_0, z_0 and the rotating spin frame associated with the local sublattice orientation is given by

$$\begin{aligned} S_i^{x_0} &= -S_i^x \sin \theta_i + \cos \theta_i (S_i^z \cos \alpha - S_i^y \sin \alpha), \\ S_i^{y_0} &= S_i^x \cos \theta_i + \sin \theta_i (S_i^z \cos \alpha - S_i^y \sin \alpha), \\ S_i^{z_0} &= S_i^y \cos \alpha + S_i^z \sin \alpha. \end{aligned} \quad (2)$$

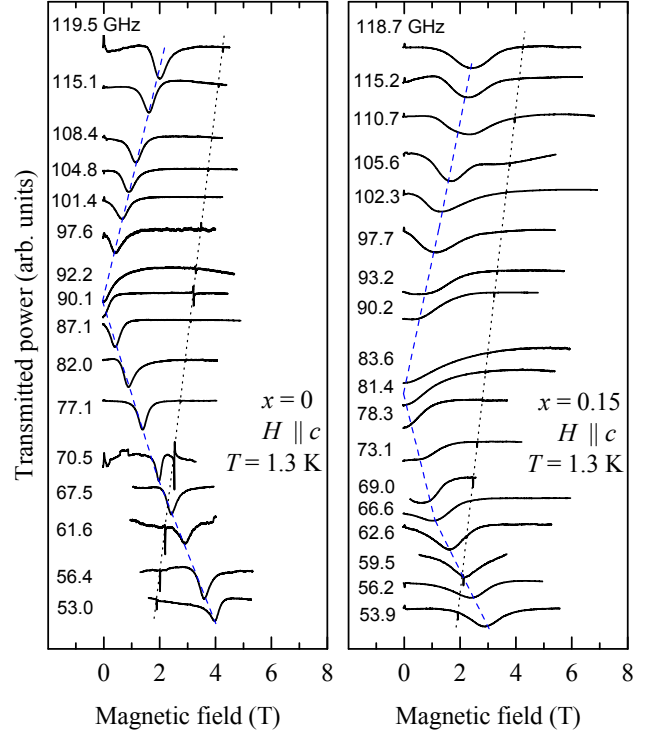


FIG. 9. Normalized ESR absorption curves for the $\text{Rb}_{1-x}\text{K}_x\text{Fe}(\text{MoO}_4)_2$ samples with $x = 0$ and 0.15 for different frequencies. Magnetic field is applied perpendicular to magnetic layers. Dashed lines are guide to the eye: blue lines are for antiferromagnetic resonance, black line is a DPPH marker.

The first two terms in the spin Hamiltonian (1) are expressed in the local frame as

$$\begin{aligned} \mathbf{S}_i \cdot \mathbf{S}_j &= -\frac{1}{2} S_i^z S_j^z (1 - 3 \sin^2 \alpha) - \frac{1}{2} S_i^x S_j^x + \\ &+ S_i^y S_j^y (1 - \frac{3}{2} \sin^2 \alpha) + (S_i^x S_j^y - S_i^y S_j^x) \sin \alpha \sin \theta_{ij} \quad (3) \\ &+ \frac{3}{4} (S_i^z S_j^y + S_i^y S_j^z) \sin 2\alpha + (S_i^z S_j^x - S_i^x S_j^z) \cos \alpha \sin \theta_{ij}, \end{aligned}$$

where we have substituted $\cos \theta_{ij} = -1/2$, and

$$\begin{aligned} (S_i^{z_0})^2 &= (S_i^z)^2 \sin^2 \alpha + (S_i^y)^2 \cos^2 \alpha + \\ &+ (S_i^z S_i^y + S_i^y S_i^z) \sin \alpha \cos \alpha. \end{aligned} \quad (4)$$

Then, the classical energy is given by

$$E_{\text{cl}}/N = -\frac{3}{2} JS^2 (1 - 3 \sin^2 \alpha) + DS^2 \sin^2 \alpha - g\mu_B HS \sin \alpha. \quad (5)$$

Minimization over the tilting angle yields $\sin \alpha = H/H_s$, where the saturation field H_s is expressed as

$$g\mu_B H_s = 9JS + 2DS. \quad (6)$$

We use the truncated Holstein-Primakoff transformation

$$\begin{aligned} S_i^x &= \sqrt{\frac{S}{2}} (a_i + a_i^\dagger), \quad S_i^y = -i\sqrt{\frac{S}{2}} (a_i - a_i^\dagger), \\ S_i^z &= S - a_i^\dagger a_i \end{aligned} \quad (7)$$

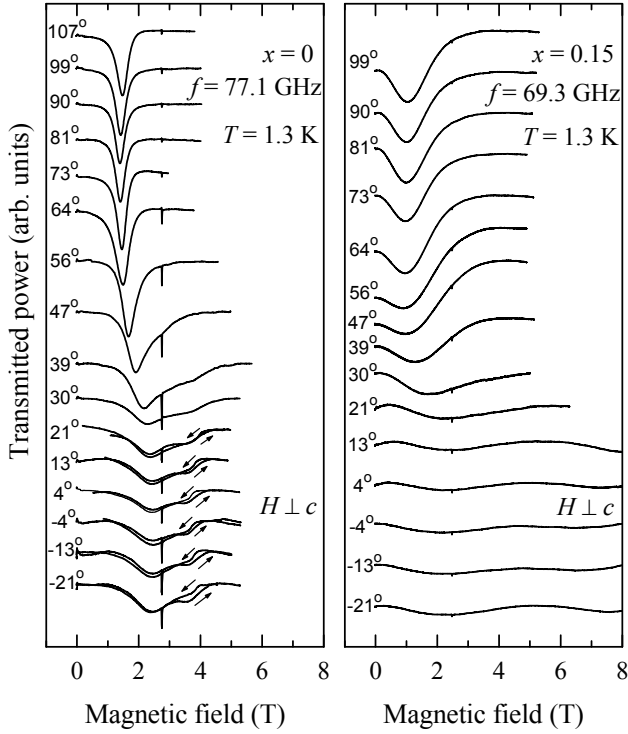


FIG. 10. Normalized ESR absorption curves for the $\text{Rb}_{1-x}\text{K}_x\text{Fe}(\text{MoO}_4)_2$ samples with $x = 0$ and 0.15 for different orientations of the magnetic field on rotation from the in-plane to normal-to-plane direction.

to obtain the harmonic spin-wave Hamiltonian. The second-order bosonic terms are

$$\begin{aligned} \hat{\mathcal{H}}_2 = & \sum_i \left\{ [g\mu_B H \sin \alpha + DS(1 - 3\sin^2 \alpha)] a_i^\dagger a_i \right. \\ & \left. - \frac{1}{2} DS \cos^2 \alpha (a_i^2 + a_i^{\dagger 2}) \right\} + JS \sum_{\langle ij \rangle} \left\{ \frac{1}{2} (1 - 3\sin^2 \alpha) \right. \\ & \times [a_i^\dagger a_i + a_j^\dagger a_j + \frac{1}{2} (a_i^\dagger a_j + a_j^\dagger a_i)] - \frac{3}{4} \cos^2 \alpha (a_i a_j + a_j^\dagger a_i^\dagger) \\ & \left. - i \sin \alpha \sin \theta_{ij} (a_i^\dagger a_j - a_j^\dagger a_i) \right\}. \end{aligned} \quad (8)$$

The Fourier transformed harmonic Hamiltonian takes the

form

$$\hat{\mathcal{H}}_2 = \sum_{\mathbf{k}} (A_{\mathbf{k}} + C_{\mathbf{k}}) a_{\mathbf{k}}^\dagger a_{\mathbf{k}} - \frac{1}{2} B_{\mathbf{k}} (a_{\mathbf{k}} a_{-\mathbf{k}} + a_{\mathbf{k}}^\dagger a_{-\mathbf{k}}^\dagger), \quad (9)$$

where

$$\begin{aligned} A_{\mathbf{k}} &= 3JS + DS \cos^2 \alpha + \frac{3}{2} JS \gamma_{\mathbf{k}} (1 - 3\sin^2 \alpha), \\ B_{\mathbf{k}} &= \frac{9}{2} JS \gamma_{\mathbf{k}} \cos^2 \alpha + DS \cos^2 \alpha, \\ C_{\mathbf{k}} &= 3JS \sin \alpha (\gamma_{\mathbf{k}+\mathbf{Q}} - \gamma_{\mathbf{k}-\mathbf{Q}}), \end{aligned} \quad (10)$$

and $\gamma_{\mathbf{k}} = \frac{1}{3} (\cos k_x + 2 \cos(k_x/2) \cos(\sqrt{3}k_y/2))$. Note, that $A_{\mathbf{k}}$ and $C_{\mathbf{k}}$ are even and odd functions of the momentum \mathbf{k} , respectively. Performing the standard Bogoliubov transformation we obtain the full magnon dispersion as

$$\epsilon_{\mathbf{k}} = \sqrt{A_{\mathbf{k}}^2 - B_{\mathbf{k}}^2} + C_{\mathbf{k}}. \quad (11)$$

The ESR modes correspond to magnons with momenta $\mathbf{k} = 0$ and $\pm \mathbf{Q}$. The former mode has zero energy $\epsilon_0 \equiv 0$ related to the continuous rotational degeneracy about the field direction. The other two modes give the ESR gaps

$$\begin{aligned} \omega_1 &= \frac{9}{2} JS \left[\sqrt{\sin^2 \alpha + (4D/9J) \cos^2 \alpha} + \sin \alpha \right], \\ \omega_2 &= \frac{9}{2} JS \left[\sqrt{\sin^2 \alpha + (4D/9J) \cos^2 \alpha} - \sin \alpha \right] \end{aligned} \quad (12)$$

that have been used to fit the experimental data for $\mathbf{H} \parallel c$ both for pure and doped samples.

As noted in the main text, for pure samples the fitting parameters are $J = 1.1J_0$ and $D = D_0$, and for $x = 0.15$ sample $J = 0.9J_0$ ($D = D_0$), in a correspondence with a reduction of the exchange interaction induced by K impurities.

-
- [1] L. E. Svistov, A. I. Smirnov, L. A. Prozorova, O. A. Petrenko, L. N. Demianets, and A. Ya. Shapiro, Phys. Rev. B **67**, 094434 (2003).
 - [2] A. I. Smirnov, H. Yashiro, S. Kimura, M. Hagiwara, Y. Narumi, K. Kindo, A. Kikkawa, K. Katsumata, A. Ya. Shapiro, and L. N. Demianets, Phys. Rev. B **75**, 134412 (2007).